JOURNAL OF GEOPHYSICAL RESEARCH, VOL. 115, D14211, doi:10.1029/2009JD013636, 2010

A new method to retrieve the aerosol layer absorption coefficient from airborne flux density and actinic radiation measurements

Eike Bierwirth,[1,2] Manfred Wendisch,[2] Evelyn Jäkel,[3] André Ehrlich,[2] K. Sebastian Schmidt,[1] Harald Stark,[4] Peter Pilewskie,[1] Michael Esselborn,[5] Gian Paolo Gobbi,[6] Richard Ferrare,[7] Thomas Müller,[8] and Antony Clarke[9]

Received 30 November 2009; revised 17 February 2010; accepted 6 April 2010; published 30 July 2010.

[1] A new method is presented to derive the mean value of the spectral absorption coefficient of an aerosol layer from combined airborne measurements of spectral net irradiance and actinic flux density. While the method is based on a theoretical relationship of radiative transfer theory, it is applied to atmospheric radiation measurements for the first time. The data have been collected with the Spectral Modular Airborne Radiation Measurement System (SMART-Albedometer), the Solar Spectral Flux Radiometer (SSFR), and the Actinic Flux Spectroradiometer (AFSR) during four field campaigns between 2002 and 2008 (the Saharan Mineral Dust Experiment (SAMUM), the Influence of Clouds on the Spectral Actinic Flux in the Lower Troposphere (INSPECTRO) project, and the Arctic Research of the Composition of the Troposphere from Aircraft and Satellites and Aerosol, Radiation, and Cloud Processes Affecting Arctic Climate (ARCTAS/ARCPAC) projects). The retrieval algorithm is tested in a series of radiative transfer model runs and then applied to measurement cases with different aerosol species and loading. The method is shown to be a feasible approach to obtain the mean aerosol absorption coefficient across a given accessible altitude range. The results indicate that the method is viable whenever the difference of the net irradiance at the top and bottom of a layer is equal to or higher than the measurement uncertainty for net irradiance. This can be achieved by a high optical depth or a low single-scattering albedo within the layer.

Citation: Bierwirth, E., et al. (2010), A new method to retrieve the aerosol layer absorption coefficient from airborne flux density and actinic radiation measurements, *J. Geophys. Res.*, *115*, D14211, doi:10.1029/2009JD013636.

1. Introduction

[2] The absorption properties of atmospheric aerosols are one of the main sources of uncertainty in assessing the contributions of aerosol particles to climate change [*Intergovernmental Panel on Climate Change*, 2007]. The targeted measurement of aerosol absorption and its spectral dependence is expressed as a research priority by NASA [*Chin et al.*, 2009] in order to reduce this uncertainty. While satellite measurements are useful to provide global coverage, satellite-based retrievals come with assumptions and restrictions that lead to inconsistencies between different instruments and algorithms, especially over land [*Kokhanovsky et al.*, 2007; *Liu et al.*, 2008]. Airborne measurements in the direct vicinity of the aerosol serve as a supplement to those methods, providing additional information albeit limited in spatial extent and global representativity. In particular, in situ probing and measurements of the solar radiation field in and around the aerosol plume give access to aerosol properties that have to be assumed in satellite retrievals. The spectral absorption properties are of particular importance because from a spaceborne point of view it is hard to distinguish aerosol absorption from variability in the underlying surface. Airborne measurements can be performed below the aerosol plume, making the distinction possible.

[3] Absorption of a medium is expressed by the absorption coefficient k_{abs} (in units of m^{-1}) which quantifies how

[1]Laboratory for Atmospheric and Space Physics, University of Colorado, Boulder, Colorado, USA.
[2]Leipziger Institut für Meteorologie, Universität Leipzig, Leipzig, Germany.
[3]Institute for Atmospheric Physics, Johannes Gutenberg University Mainz, Mainz, Germany.
[4]Earth System Research Laboratory, NOAA, Boulder, Colorado, USA.
[5]Institut für Physik der Atmosphäre, Deutsches Zentrum für Luft- und Raumfahrt, Oberpfaffenhofen, Germany.
[6]Institute of Atmospheric Sciences and Climate, CNR, Rome, Italy.
[7]NASA Langley Research Center, Hampton, Virginia, USA.
[8]Leibniz Institute for Tropospheric Research, Leipzig, Germany.
[9]School of Ocean and Earth Science and Technology, University of Hawai'i at Mānoa, Honolulu, Hawaii, USA.

0148-0227/10/2009JD013636

strongly radiation is attenuated because of absorption in the medium,

$$I = I_0 \cdot \exp(-k_{\text{abs}} \cdot s) \tag{1}$$

(where I_0 is incident radiance, I is radiance after passing the medium, and s is the path distance in the medium). The radiation is also attenuated by scattering; the total loss is expressed by the extinction coefficient, k_{ext}. The fraction of extinction that is caused by scattering is expressed by the unitless single-scattering albedo $\omega_0 \in [0,1]$. While ω_0 compares absorption and scattering by a given aerosol type independent of its concentration in the atmosphere, the absorption and extinction coefficients quantify the radiative effects of a real aerosol plume and are necessary to define the total absorbed radiation by a layer. They are connected by the formula

$$k_{\text{abs}} = (1 - \omega_0) \cdot k_{\text{ext}}. \tag{2}$$

The wavelength dependence is commonly approximated by a power law $\lambda^{-\alpha}$ with an Ångström exponent α. The Absorption Ångström Exponent (AAE) can be used to distinguish different aerosol species [*Bergstrom et al.*, 2007]: black carbon has an AAE of 1, other carbonaceous aerosols (urban, biomass burning) have values between 1 and 2, and mineral dust 2 or larger. Airborne measurements of the aerosol absorption coefficient are most commonly performed in situ, e.g., with a Particle Soot Absorption Photometer (PSAP) with aerosol particles being collected in the aircraft cabin. Measurements with these kinds of instruments are limited to the actual flight altitude of the aircraft. Furthermore, the particle absorption coefficient can be underestimated if the particle inlet cuts off large particles. This can be a serious issue, for instance, in desert dust aerosol where large particles are abundant and relevant for the overall absorptivity of the aerosol [*Otto et al.*, 2009]. In addition to that, knowledge or an estimate of the aerosol scattering coefficient is also required for data processing [e.g., *Bond et al.*, 1999; *Virkkula et al.*, 2005].

[4] Radiation measurements offer an alternative pathway to investigate the optical properties of an aerosol without direct contact, that is without the technical limitations of in-flight particle sampling. If the irradiance is measured at the top and the bottom of an aerosol layer, its absorption can be estimated in terms of absorbed irradiance (also called flux divergence, defined as the difference of net irradiances at top and bottom of that layer); or in terms of fractional absorption, which is the absorbed irradiance divided by the downwelling irradiance at the layer top [e.g., *Bergstrom et al.*, 2003; *Pilewskie et al.*, 2003]. However, the absorption coefficient in units of inverse meters cannot be retrieved this way without a model-based retrieval. Other objectives of irradiance measurements include radiative forcing studies [e.g., *Haywood et al.*, 2001; *Redemann et al.*, 2006; *Schmidt et al.*, 2009] and the retrieval of surface albedo [e.g., *Webb et al.*, 2004; *Wendisch et al.*, 2004; *Coddington et al.*, 2008; *Bierwirth et al.*, 2009].

[5] It is desirable to derive the actual aerosol absorption coefficient from radiation measurements, i.e., without the problems involved with particle sampling. A possible pathway to this has been outlined by *Chandrasekhar* [1960]. For this method it is necessary to measure an additional radiative quantity, the actinic flux density

$$F_{\text{act}} = \int_{4\pi} I(\Omega)\, \mathrm{d}\Omega. \tag{3}$$

Its definition differs from that of irradiance in that the latter contains a weighting with the cosine of the angle of incidence in the integral. The actinic flux density is commonly measured to derive chemical photolysis rates [e.g., *Wendisch et al.*, 1996; *Früh et al.*, 2000; *Kanaya et al.*, 2003; *Jäkel et al.*, 2006; *Stark et al.*, 2007], and for obtaining aerosol heating rates [*Gao et al.*, 2008]. The different objectives for measuring irradiance and actinic flux density do not often lead to a simultaneous measurement of both quantities. However, if combined measurements are performed, it is feasible to derive the absorption coefficient of an atmospheric layer by measuring the net irradiance and the actinic flux density at the top and at the bottom of this layer. If a vertical extinction profile is available, as commonly provided by a high spectral resolution lidar (HSRL) or Raman lidar, then the average single-scattering albedo of the aerosol particles in the layer is also accessible by virtue of equation (2).

[6] In this paper, this method is derived from the divergence form of the Equation of Transfer [*Chandrasekhar,* 1960]. Section 2 of this paper outlines how this equation can be applied to real measurements, and this is tested for modeled cases, as presented in section 3. Section 4 describes the instrumentation we used for the radiation measurements, the retrieval uncertainty, and accommodations for time synchronization problems that are particular to field data. Results from the different field campaigns are presented in section 5.

2. Methodology

[7] *Chandrasekhar* [1960, equation 56] derives from the radiative transfer equation in a scattering and absorbing atmosphere that

$$\frac{1}{4\kappa^{\text{m}} \cdot \rho} \mathrm{div} F^{\text{C}} = (1 - \omega_0) \cdot J, \tag{4}$$

where κ^{m} is the mass extinction coefficient and ρ is the density of the medium. In our case, the medium is an aerosol, i.e., air plus particles. In order to use equation (4), we need to adjust Chandrasekhar's terminology to modern conventions (note that Chandrasekhar used the term absorption for what we now call extinction, made up of scattering and "true absorption"). F^{C} is the "net flux" in Chandrasekhar's definition; it is equal to the net irradiance F divided by π. J is the "average intensity" which is the actinic flux density divided by 4π.

[8] Using these relations, and merging the density with the mass extinction coefficient to obtain the volumetric extinction coefficient k_{ext} (in units of m^{-1}), we rewrite equation (4) in terms of net irradiance F (which in our two-dimensional approach is downwelling minus upwelling irradiance) and actinic flux density F_{act},

$$\nabla F = k_{\text{ext}} \cdot (1 - \omega_0) \cdot F_{\text{act}} = k_{\text{abs}} \cdot F_{\text{act}}. \tag{5}$$

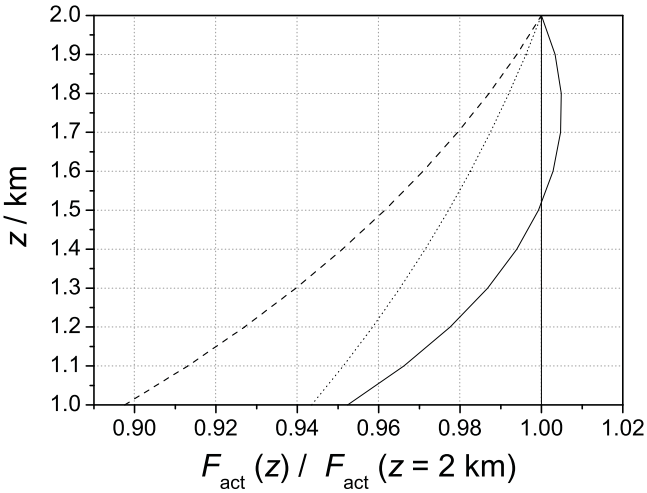

Figure 1. Actinic flux density F_{act} within an aerosol layer that is located in an otherwise clear atmosphere. Solid and dotted curves are the dust layer between 1 and 2 km altitude, with ω_0 of 1.0 and 0.8, respectively. The dashed curve is $\omega_0 = 0.96$, but the aerosol layer extends from 0 to 4 km. The vertical solid line is for orientation only.

[9] We now apply equation (5) to the practical case of a horizontally homogeneous layer, such that $\frac{\partial}{\partial x} = \frac{\partial}{\partial y} = 0$. Assuming that airborne radiation measurements of F and F_{act} are performed at the bottom and the top of this layer at altitudes z_1 and z_2, respectively, the vertical integration of equation (5) leads to

$$\int_{z_1}^{z_2} \frac{\partial F}{\partial z} \mathrm{d}z = F(z_2) - F(z_1) = \overline{k_{abs}} \int_{z_1}^{z_2} F_{act} \mathrm{d}z, \qquad (6)$$

where $\overline{k_{abs}}$ is the mean absorption coefficient of the layer between z_1 and z_2.

[10] If the vertical profile of F_{act} is not available (e.g., from a spiral descent at the same location), then the right side integral can be numerically approximated by an auxiliary radiative transfer model, constrained by the F_{act} measurements at z_1 and z_2. The integral cannot be replaced by a mean value because the vertical behavior of the actinic flux density within the layer cannot be generally assumed to be linear or even monotonic. An example for the vertical behavior is shown in Figure 1: an observer descending into a weakly or nonabsorbing aerosol layer would detect an initial increase in F_{act}. The behavior changes to a straight decrease deeper within the layer or if absorption is high. As a consequence, this step requires some knowledge or reasonable assumptions about the atmospheric structure. In all presented cases, however, such information was available from independent measurements, e.g., by lidar techniques.

[11] We have to distinguish between the properties of the entire aerosol (which includes air molecules) and those of the aerosol particles (such as mineral dust, soot, ice crystals, etc.), both of which contribute to the volumetric absorption coefficient. In our wavelength and altitude range, the absorption coefficients of the aerosol and the particles alone are practically identical with the exception of the spectral bands where ozone and water vapor molecules absorb radiation. In this paper we correct for molecular absorption and report the absorption coefficients of the aerosol particles only.

3. Test Simulations

[12] In order to test our methodology, we employ the radiative transfer model DISORT2 [*Stamnes et al.*, 1988] implemented in the software package *libRadtran* [*Mayer and Kylling*, 2005], version 1.4, using six streams and a US standard atmosphere, into which we placed an aerosol layer with adjustable properties. The model calculates the net irradiance F and the actinic flux density F_{act} at the two altitudes chosen for the simulated measurements, plus 18 additional intervening altitudes for the actinic flux density integration. From the calculated quantities, $\overline{k_{abs}}$ is derived according to equation (6), and compared to the input, i.e., to $k_{ext} \cdot (1 - \omega_0)$. Absorption by gas molecules is taken into account by subtracting the result of an additional aerosol-free model run. The relative difference between the modeled net irradiance at top and bottom altitudes provides a measure of the measurement accuracy required to detect the change in radiation caused by the layer absorption.

[13] The test scenarios assume an aerosol layer that is 1 km thick, and in each test one quantity is varied while the others are kept at default values that are based on data measured during the Saharan Mineral Dust Experiment (SAMUM) field campaign in Morocco (extinction coefficient 0.3 km^{-1}, single-scattering albedo 0.96, asymmetry parameter g 0.75, surface albedo 0.2, bottom of layer at 2 km altitude). The wavelength is 550 nm. Table 1 shows the resulting absorption error (relative difference between input and output absorption coefficient) as well as the relative difference of net irradiances between the upper and lower altitudes.

[14] In all modeled scenarios the derived $\overline{k_{abs}}$ agreed with the model input to better than 0.1% (except for cases with very low AOD) which shows that the algorithm replicates *Chandrasekhar*'s [1960] theoretical formula. The slight but nonzero discrepancy is mostly due to computation errors while differencing two large numbers of similar magnitude.

Table 1. Influence of Aerosol Particle Properties and of the Surface Albedo ρ on the Retrieval Error of the Mean Particle Absorption Coefficient of the Aerosol Layer and on the Difference of Net Irradiances dF_{net} at the Top and Bottom of the Layer[a]

Property	dk_{abs} (%)	dF_{net} (%)
AOD = 0.1	0.2	0.8
AOD = 0.5	0.005	4.3
AOD = 1.0	0.01	9.3
AOD = 2.0	0.03	22
$\omega_0 = 0.5$	−0.003	29
$\omega_0 = 0.8$	0.001	12
$\omega_0 = 0.96$	0.005	2.5
$g = -0.75$	0.007	2.6
$g = 0.0$	0.01	3.0
$g = 0.75$	0.005	2.5
$g = 0.90$	0.01	2.4
$\rho = 0.0$	0.006	1.7
$\rho = 0.5$	0.003	5.4
$\rho = 0.9$	0.002	35

[a]Aerosol particle properties are AOD, single-scattering albedo ω_0, and asymmetry parameter g. Mean particle absorption coefficient of the aerosol layer is expressed as the relative difference dk_{abs} of model input and retrieved value.

Table 2. Technical Parameters of the Spectrometers Used for This Study

Type[a]	λ/μm	Number of Pixels	FWHM/μm	Quantity[b]
		SMART-Albedometer		
MCS 55 UV/VIS	290–1000	1024	2–3	irradiance
PGS NIR 2μ2	900–2200	256	9–16	irradiance
MCS UV/VIS	280–700	512	2–3	actinic flux density
		SSFR		
MMS-1	350–1000	256	10–15	irradiance
PGS NIR 2μ2	900–2200	256	9–16	irradiance
		AFSR		
PI SP-150	280–490	400	1–2	actinic flux density
AR INS 150-250B	460–689	256	1–2	actinic flux density

[a]MCS, MMS, and PGS stand for Zeiss' Multichannel Spectrometer, Monolithic Miniature Spectrometer, and Plane Grating Spectrometer, respectively. PI is Princeton Instruments and AR is Acton Research.
[b]Upwelling and downwelling component measured for each quantity.

[15] The tests show that high AOD and low single-scattering albedo are favorable for this technique, because this increases the difference in net irradiance. A high surface albedo is also helpful because of an increased probability of photon interaction with the aerosol particles. The influence of g is generally much lower than that of the other quantities. In an additional test, the elevation of the layer is changed between 0 and 10 km but this has no influence on the retrieval.

4. Application to Atmospheric Measurements

4.1. Time Correction

[16] The largest obstacle in applying equation (6) to airborne measurements is the time difference between the measurements at the two altitudes when only one aircraft was deployed, as in most cases investigated here. First, one has to verify that the aerosol conditions do not change during the time the measurements are acquired. Second, the change of the solar zenith angle with time leads to changes in the radiation field that may easily exceed those due to absorption. In order to correct for the latter effect, the auxiliary radiative transfer model (again, DISORT2 in *libRadtran*) is employed to simulate the radiation field at all four combinations of altitudes z_1, z_2 and times t_1, t_2. The ratios of the modeled irradiance and actinic flux density are used to extrapolate the measurements at (z_1, t_1) to (z_1, t_2) and those at (z_2, t_2) to (z_2, t_1). This concept requires that the aerosol is the same at t_1 and at t_2 but yields the necessary data at both altitudes and at both times.

4.2. Instruments

[17] Three airborne spectrometer systems have been used in the experiments investigated in this study. The Spectral Modular Airborne Radiation Measurement System, or SMART-Albedometer, developed and operated by the Leibniz Institute for Tropospheric Research (IfT) in Leipzig and the University of Leipzig [see *Wendisch et al.*, 2001; *Bierwirth*, 2008], measures upwelling and downwelling irradiance and actinic flux density. It was deployed in the experiments of 2002, 2004, and 2006, and makes use of fixed grating, photodiode array spectrometers manufactured by Zeiss (Jena, Germany). The Solar Spectral Flux Radiometer (SSFR) of the Laboratory for Atmospheric and Space Physics (LASP) in Boulder, USA [*Pilewskie et al.*, 2003] measures upwelling and downwelling irradiance with a very similar set of spectrometers. The Actinic Flux Spectroradiometer (AFSR) uses CCD spectrometers (manufactured by Princeton Instruments, Trenton, New Jersey, and Acton Research, Acton, Massachusetts), with a detailed description given by *Stark et al.* [2007]. The combination of these two systems was deployed in the 2008 experiment. More detailed specifications of these systems are summarized in Table 2.

[18] Irradiance is measured by these systems using optical inlets that are based on the design of *Crowther* [1997]. An integrating sphere with a cone baffle diffuses the incoming light weighted by the cosine of the angle of incidence, as required by the definition of irradiance. Deviations from the ideal cosine behavior are corrected for by using lab calibrations.

[19] The actinic flux density is measured by smoked (SMART-Albedometer) or sand-blasted (AFSR) quartz domes that collect radiation without any directional dependence [*Jäkel et al.*, 2005; *Stark et al.*, 2007]. Optical fibres transmit the signal from both types of detectors (mounted on top and/or bottom of the aircraft fuselage) to the spectrometers in the cabin.

[20] Measurements of upwelling and downwelling irradiance rely on a clear distinction between photons from the upper and the lower hemispheres, especially if the instrument is mounted on a moving aircraft. For this, the optical inlets of the SMART-Albedometer are mounted on a stabilization platform, built by enviscope GmbH (Frankfurt, Germany) which keeps the inlets horizontally aligned within 0.2° for roll and pitch angles of the aircraft of up to 6° [*Wendisch et al.*, 2001]. As the SSFR operates without such a platform, the data are corrected after the experiment using the recorded roll and pitch values of the aircraft.

4.3. Expected Uncertainty

[21] The absolute uncertainty of the retrieved layer absorption coefficient is dominated by the uncertainty in the difference between the net irradiance at the top and bottom altitudes of the layer because it is a small difference of two much larger numbers. Error propagation for equation (6) leads to

$$u\left(\overline{k_{\mathrm{abs}}}\right) = \overline{k_{\mathrm{abs}}} \cdot \left(\frac{2u(F)}{F(z_2) - F(z_1)} + \frac{u(F_{\mathrm{act}})}{\int_{z_1}^{z_2} F_{\mathrm{act}} \mathrm{d}z} \right), \qquad (7)$$

where $u(x)$ denotes the (absolute) uncertainty of the quantity x. For illustration, we performed a series of radiative transfer model runs (same model as in section 3) for an aerosol layer with varying AOD. The model aerosol layer extended from 1 to 3 km altitude (where also the model output was taken), with $g = 0.75$ and $\omega_0 = 0.96$. The surface albedo was set to 0.2, the wavelength was 550 nm. The retrieval uncertainty is calculated using the measurement uncertainties of the SMART-Albedometer (4.5% for net irradiance, 4.9% for actinic flux density) which are similar to those of the SSFR, given as 3%–5% for irradiance over its spectral range

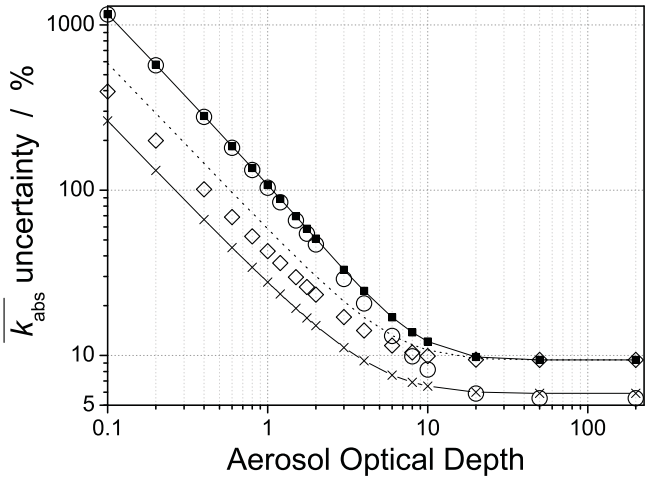

Figure 2. Dependence of the uncertainty of the retrieved $\overline{k_{abs}}$ according to equation (7) on the basis of a modeled radiation field, calculated at 550 nm wavelength. Solid squares show the retrieval uncertainty assuming radiation measurement uncertainties of the SMART-Albedometer: 4.5% for F and 4.9% for F_{act} (Case A0). The diamonds show Case A0b for a more absorbing aerosol (ω_0 = 0.88 instead of 0.96). The crosses show Case A1, a hypothetical instrument which measures F with 1% uncertainty but F_{act} as above; the circles show an instrument which measures F_{act} with 1% uncertainty but with the original irradiance uncertainty (Case A2). The dotted line shows Case B, the optimistic error estimate.

[*Coddington et al.*, 2008], and to those of the AFSR of 5% [*Stark et al.*, 2007]. We call this Case A0. The resulting $\overline{k_{abs}}$ uncertainties, shown in Figure 2, extend beyond 1000% for optically thin layers (AOD around 0.1) and decrease to 100% at an AOD of 1, which is in the range of heavily polluted conditions. It converges to about 9% (twice the uncertainty of the net irradiance) for cases of high optical depths encountered only in clouds. For most aerosol layers, we can therefore expect uncertainties that are of the same order of magnitude as the retrieved absorption coefficient itself. A test with a stronger absorbing aerosol (ω_0 = 0.88) but otherwise identical conditions, Case A0b, shows a strong reduction of the error by a factor of 2–3 for AODs of up to 1, which is in agreement with section 3. Again, it converges to 9% for higher AODs.

[22] In another model test (Case A1), also shown in Figure 2, we simulated an instrument with a reduced net irradiance uncertainty of 1%. The resulting uncertainty of the particle absorption coefficient is significantly reduced, although it still reaches hundreds of percents for weakly absorbing layers. A simulation of an instrument that has 1% uncertainty for actinic flux density but 4.5% for net irradiance (Case A2) shows only little improvement.

[23] This behavior is evident from equation (7). The first term (irradiance contribution) increases without bound for $F(z_2) - F(z_1) \rightarrow 0$, amplifying the irradiance measurement uncertainty of the instrument. In consequence, any improvement in irradiance uncertainty is also amplified. In contrast, the second term (actinic flux density) does not behave critically for any situation (except darkness) which also means that a reduction of the F_{act} uncertainty propagates without amplification. The conclusion is that accurate results can only be obtained if the change in net irradiance (at the two levels) is larger than the measurement uncertainty for net irradiance.

[24] In equation (7) it is assumed that the difference of two net irradiances has twice the uncertainty of the net irradiance, which means that the uncertainty of $F(z_1)$ is independent of the $F(z_2)$ uncertainty. However, in practice both measurements have been performed by the same instrument (or in the Arctic Research of the Composition of the Troposphere from Aircraft and Satellite (ARCTAS) case by instruments that have been calibrated with the same irradiance standard). Therefore, some contributions to $u(F)$ cancel when the difference is taken. Taking this into account replaces the factor 2 in equation (7) by some unknown factor between 1 and 2. Instead of attempting to quantify it, we set it to 1 and take the result as the limiting optimum value, i.e., the measurement uncertainty under most favorable conditions. We call this Case B; the uncertainties for this case are also shown in Figure 2. For typical AODs of 1 or less, this optimistic limit leads to an uncertainty reduction by a factor of 2. With increasing AOD there is less improvement, because the difference of net irradiance is not as small and therefore less critical.

[25] Additionally, there are contributions to the uncertainty in $\overline{k_{abs}}$ from the optical properties of the aerosol particles that are used to run the auxiliary radiative transfer model. However, we found this influence to be small compared to that of the radiation measurement uncertainties. If we change the single-scattering albedo in the auxiliary model by 10%, then the single-scattering albedo that is retrieved from the radiation measurements changes by less than 2%. The remaining model parameters have even less influence. That means that the retrieval results depend primarily on the measurements themselves and are not predetermined by the input parameters of the auxiliary model, which is an important prerequisite for this measurement-based technique.

[26] In order to test the prerequisite that the aerosol does not change between the two measurements at the two altitudes, we use the radiative transfer model to simulate a measurement case in which the AOD of the probed layer changes during the time between the measurements at top and bottom of the layer (Figure 3). It turns out that only very large changes in AOD cause notable changes in the retrieved absorption coefficient. For example, an AOD of 0.2 that (undetected) changes by 10% would lead to an error in $\overline{k_{abs}}$ of 1%. An AOD of 0.6 that changes by 10% would lead to an error of 2%. As AOD changes of this magnitude have not been observed in the cases investigated in this study, we conclude that the requirement of constant aerosol conditions is met well enough with little or no impact on the retrieval results.

[27] During the data processing we experienced that the irradiance measurements are significantly improved by the use of a horizontal stabilization platform. The effort to calibrate the ARCTAS/ARCPAC (Aerosol, Radiation, and Cloud Processes Affecting Arctic Climate) irradiance data was much larger than for the other experiments because of the lack of such a platform. This shows us again that the efforts in building and operating a stabilizing platform for

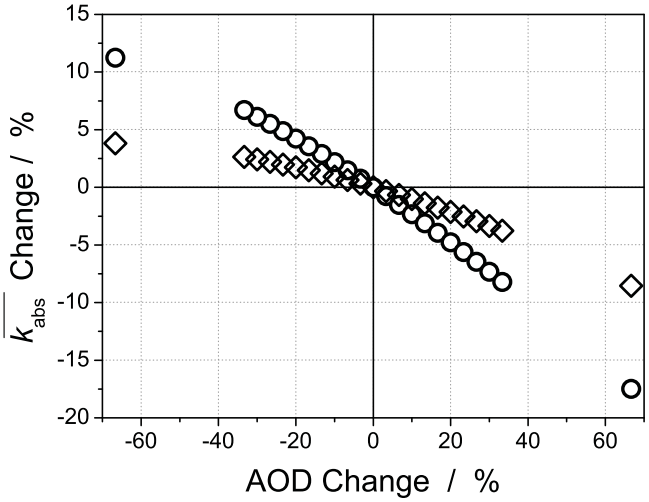

Figure 3. Modeled k_{abs} error caused by AOD changes that occur undetected while the aircraft flies from the lower measurement point to the upper one. The model assumes an aerosol layer at 1–3 km altitude, $\omega_0 = 0.96$, $g = 0.75$, and surface albedo 0.2. Two cases are shown: initial AOD 0.6 (circles) and 0.2 (diamonds).

the radiation sensors are more than compensated by gains in data quality.

5. Results

5.1. SAMUM, Morocco 2006

[28] SAMUM was conducted by a consortium of German research institutes in southeastern Morocco in May and June 2006 [*Heintzenberg,* 2009]. The SMART-Albedometer was installed on a Partenavia P68B aircraft (call sign D-GERY) and measured upwelling and downwelling irradiance in the wavelength range 250–2100 nm, and actinic flux density from 280 to 700 nm. The Falcon aircraft of the German Aerospace Center (D-CMET) cruising at higher altitudes carried a high spectral resolution lidar (HSRL) which provided vertical profiles of the aerosol particle extinction coefficient [*Esselborn et al.*, 2009]. The aerosol optical depth (AOD) was monitored by a CIMEL Sun photometer at the Tinfou ground site at 30.24°N, 5.61°W [*von Hoyningen-Huene et al.*, 2009]. In addition, spectra of the aerosol particle absorption (15% uncertainty) measured by the Spectral Optical Absorption Photometer (SOAP) at Tinfou are used for comparison [*Müller et al.*, 2009]. Furthermore, scattering coefficients measured with an integrating nephelometer and absorption coefficients measured with a PSAP (Particle Soot Absorption Photometer) and MAAP (MultiAngle Absorption Photometer) are used. Because of sampling lines of different length and bending losses, the sampling efficiencies of these instruments differ. The SOAP was placed directly beneath a PM_{10} inlet thus no more sampling losses are expected. Absorption and scattering coefficients measured with nephelometer, PSAP, and MAAP have been corrected for sampling line losses. A detailed description of the correction is given by *Schladitz et al.* [2009]. Thus the optical properties given for the in situ measurements correspond to PM_{10}. The probed aerosol contained primarily mineral dust from the Sahara [*Knippertz et al.*, 2009].

[29] For this study, data of the morning flight on 3 June 2006 was chosen (0800–0835 UTC) because both aircraft operated in the same area, and the AOD is reported to be almost constant during this period. The latter is supported by HSRL scans of the aerosol distribution which is horizontally homogeneous in the probed region and at the altitudes in question, so no significant changes due to advection are expected. The aircraft location was 30.23°N, 6.08°W. The measurement at lower altitude (300 m above ground level (AGL)) was performed at 0833:47 UTC and that at high altitude (2300 m AGL) at 0804:25 UTC. The corresponding solar zenith angles were 51.3° and 57.7°. The extinction profile measured by the HSRL (Figure 4) shows a thick aerosol layer below 2 km AGL and a thinner second layer that peaks at 3.2 km AGL. The total integral of this profile corresponds to an AOD of 0.52 at 532 nm, of which 0.42 were located between the Partenavia flight altitudes. The Ozone Monitoring Instrument (OMI) [*Levelt et al.* 2006] reports the ozone column to be 300 DU.

[30] The first step of the retrieval is to perform the temporal extrapolation to correct for the change in solar zenith angle that occurred between the two measurements. The surface albedo that is used for all model runs is extracted from the irradiance data with the algorithm as described by *Bierwirth* [2008] on the basis of the scheme proposed by *Wendisch et al.* [2004]. The resulting corrected spectra of net irradiance (Figure 5) show a large difference between the two altitudes, with changes ranging between 6.5% and 15% (depending on wavelength) which indicates a significant absorption signal.

[31] The spectral mean absorption coefficient obtained by the new method is presented in Figure 6. Results are shown only at wavelengths above 320 nm because of diminished signal-to-noise ratio at shorter wavelengths. With the help of the HSRL extinction profile (Figure 4), the mean single-scattering albedo $\overline{\omega_0}$ of the dust layer can be derived from $\overline{k_{abs}}$, shown in Figure 6 as a dashed line. The spectral behavior of $\overline{k_{abs}}$ with an Absorption Ångström Exponent (AAE) (at wavelengths 350 and 500 nm) of 3.4 clearly indicates mineral dust [*Bergstrom et al.*, 2007]. Only the

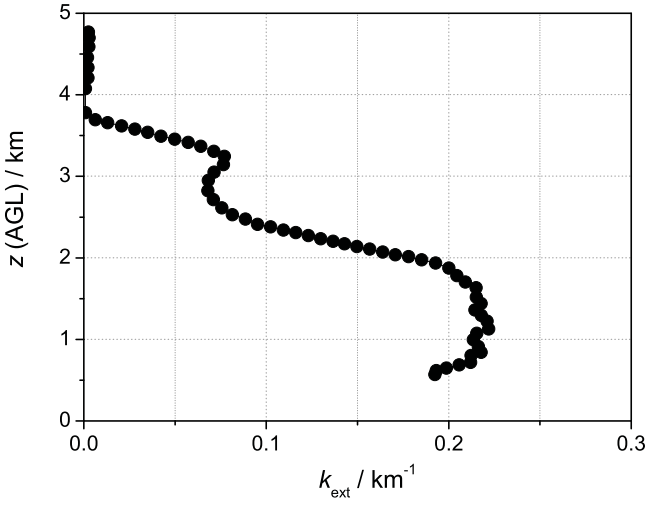

Figure 4. Aerosol extinction profile measured during SAMUM in the western Zagora basin on 3 June 2006 by the HSRL on the Falcon aircraft.

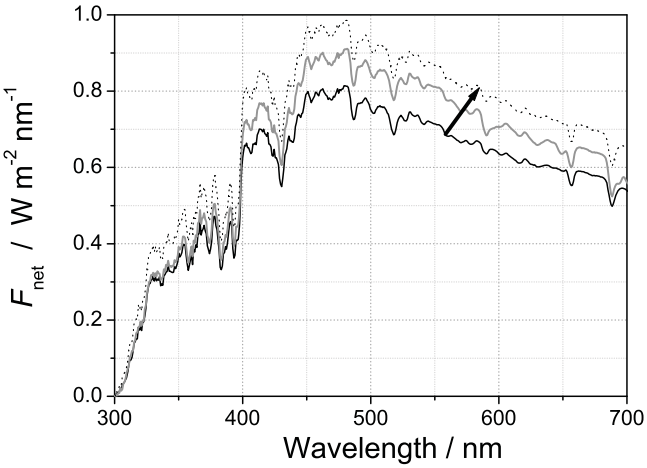

Figure 5. Temporal extrapolation of net irradiance from SAMUM measurements on 3 June 2006 to correct for the change of solar zenith angle. The measurement at the top of the dust layer (black solid line) was performed at 0804 UTC, earlier than the measurement at the layer bottom at 0833 (grey solid line). The dotted line is the net irradiance that would have been measured at the top of the layer at 0833.

increase beyond 500 nm is atypical. The increase of $\overline{\omega_0}$ with wavelength and its value near 0.95 is also typical, while the decrease at wavelengths longer than 570 nm is not (caused by $\overline{k_{abs}}$).

[32] When comparing the retrieved spectrum of $\overline{k_{abs}}$ to that derived from SOAP measurements (Figure 7), we find a similar spectral behavior for wavelengths up to 500 nm. Toward longer wavelengths, the SOAP data decline further while the retrieved $\overline{k_{abs}}$ remains constant and even increases a little. This behavior is likely a measurement artifact as the absorption signal in the radiation field gets low at longer wavelengths. The comparison also shows that the retrieved absorption coefficients are larger than the SOAP data by a factor of 1.2–1.5. This can be explained by the influence of large dust particles: a summary by *Otto et al.* [2009, section 5.2] of single-scattering albedo values from various studies shows that they are lower (0.77–0.90) when coarse particles are included, and higher (0.90–0.95) without coarse particles. From this we estimate that neglecting the large particles in the Saharan dust plume can lead to an underestimation of absorption by a factor of up to 4.6 (in extreme cases). The inlet that feeds the aerosol to the SOAP and to the nephelometer did not sample particles larger than 10 μm aerodynamical diameter; however, chemical analysis indicates that particles of up to 40–50 μm diameter were advected from Tunisia on 3 June 2006 [*Kandler et al.*, 2009] and may explain the observed difference. Even larger particles of up to 100 μm and beyond have been observed at the Tinfou ground station, but those stem from local sources and are limited to near the surface. They are therefore irrelevant for the given comparison. The single-scattering albedo derived from ground-based in situ measurements at the Tinfou site (diamonds in Figure 6) is higher than the retrieved values which is due to the overestimated retrieved absorption coefficient.

5.2. INSPECTRO, United Kingdom 2002 and Germany 2004

[33] Two fields campaigns were conducted during the influence of clouds on the spectral actinic flux in the lower troposphere (INSPECTRO) project, the first in East Anglia, United Kingdom, in September 2002, and the second near Straubing, Germany, in May 2004. The SMART-Albedometer was installed on the Partenavia P68B aircraft to measure upwelling and downwelling irradiance (250–1000 nm) and actinic flux density (280–700 nm). An overview of the campaigns has been given by *Kylling et al.* [2005] and *Thiel et al.* [2008]. Two cases are analyzed in this study: profiles flown on 12 September 2002 and on 20 May 2004. The vertical profile of the extinction coefficient was measured by the Vehicle-Mounted Lidar System VELIS [*Gobbi et al.*,

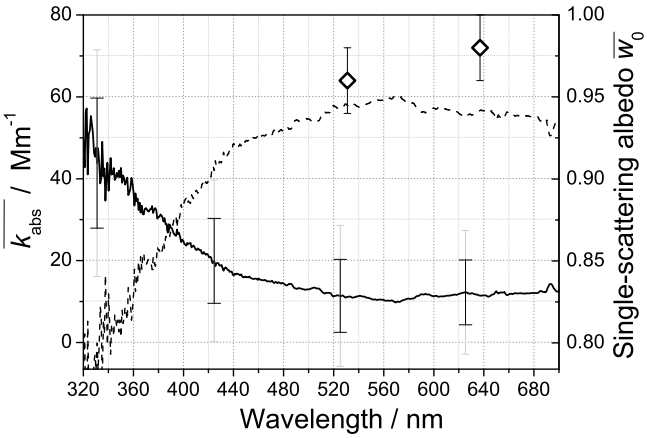

Figure 6. Retrieved absorption coefficient $\overline{k_{abs}}$ (solid line) and single-scattering albedo (dashed line) for the SAMUM case, Saharan mineral dust in Morocco. Diamonds are single-scattering albedo derived from ground-based (Tinfou) absorption coefficients (PSAP 525 nm and MAAP 637 nm) and scattering coefficients measured by a nephelometer.

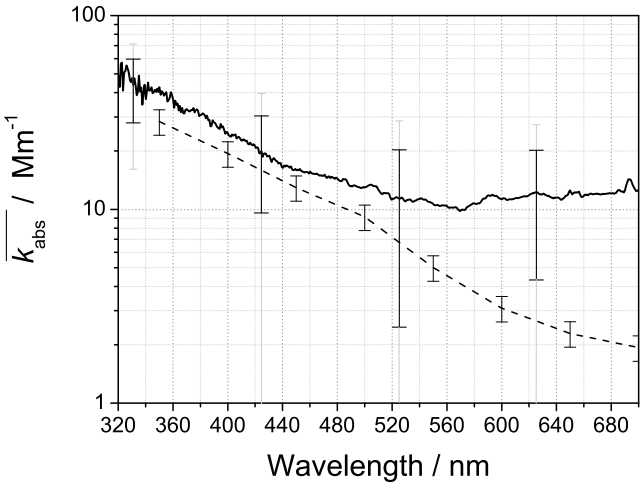

Figure 7. Comparison (log scale) of the absorption coefficient retrieved from airborne radiation measurements (solid line) to that measured by SOAP with a PM10 inlet at the Tinfou ground site (dashed line) with error bars showing the 15% uncertainty.

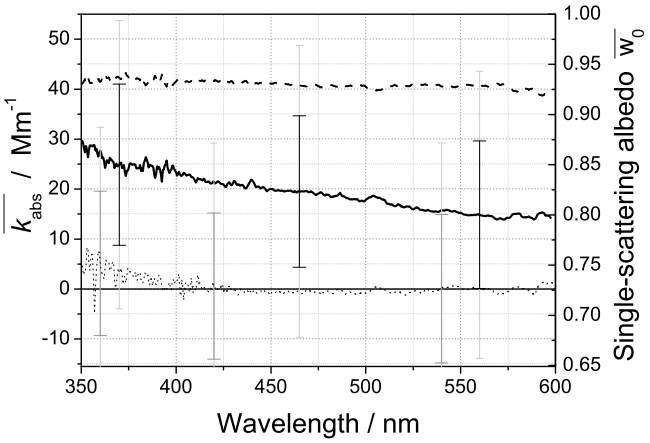

Figure 8. Retrieved mean absorption coefficient (solid line) and mean single-scattering albedo (dashed line) for INSPECTRO Germany, 20 May 2004. Additionally, $\overline{k_{abs}}$ retrieved for the United Kingdom flight, 12 September 2002, is shown by the dotted line (near zero) with grey error bars.

2000]. The Earth Probe Total Ozone Monitoring Spectrometer (TOMS) [*Hudson et al.*, 1995] yielded the ozone column as 269 DU for the 2002 case, and 346 DU for the 2004 case.

[34] The flight on 12 September 2002 included a descending profile that showed only weak changes in the measured radiation quantities. While the actinic flux density changed by 29% during the descent, the net irradiance changed only by 1% which is far below the measurement uncertainty of 4.5%, so we expect to retrieve a null absorption signal in this case. The profile was conducted between 1325 and 1336 UTC, starting at 1258 m AGL and ending over Norwich Airport (52.68°N, 1.26°E) at 72 m. The total AOD obtained from the VELIS lidar was 0.11 at 532 nm, most of which was concentrated in the boundary layer below 1–2 km altitude. The probed layer contributed 0.08. The aerosol was a low-absorbing maritime type (single-scattering albedo of 0.98, northerly winds) [see *Kylling et al.*, 2005]. The retrieved mean absorption coefficient for this case (included in Figure 8) is very low and at some wavelengths negative. Such a nonphysical result indicates that it is influenced by uncertainties in the temporal extrapolation more than by absorption, so this is a case where the aerosol absorption is too weak to be detected in the uncertainty range of our instrumentation. Only the weak absorption signal at wavelengths below 375 nm may be caused by actual absorption, due to the increase of AOD with decreasing wavelength.

[35] On the flight of 20 May 2004 there were no clouds but a relatively high AOD. The analyzed profile is a descent from the top of the boundary layer near Straubing (0802:10 UTC, 48.72°N, 12.78°E, 1950 m AGL) to Fürstenzell (0810:14 UTC, 48.50°N, 13.11°E, 737 m AGL). The change in net irradiance between the two altitudes ranged between 5% and 10% depending on wavelength, higher than the measurement uncertainty of the SMART-Albedometer. Downwelling actinic flux density, and therefore all retrieved quantities, are available only up to 600 nm wavelength for this day. The VELIS lidar operated in nearby Buchhofen. It recorded a total AOD of 0.31 at 532 nm which is lower than that observed by the colocated Microtops Sun photometers (0.62, 0.48, 0.18 at 440/500/1020 nm; Ångström exponent 1.55) because of aerosol located below the range detectable by the lidar. Therefore, we use the total AOD data from the Microtops Sun photometers. The lidar profile gives the AOD of the probed layer (between 737 and 1950 m AGL) as 0.17–0.19.

[36] Figure 8 shows the retrieved mean absorption coefficient and the single-scattering albedo derived from $\overline{k_{abs}}$ (using a mean extinction coefficient estimated by the observed spectral AOD and a boundary layer height of 1.95 km). No independent absorption measurements are available for this case, but the Absorption Ångström Exponent of 1.4 (350 and 600 nm) indicates carbonaceous aerosol with certain organic mass fraction (as it is not close to 1 as it would be for purely industrial aerosol), possibly due to biomass burning. This seems possible as a HYSPLIT air mass back trajectory [*Draxler and Hess*, 1998] and the MODIS Rapid Response fire detection [*Giglio et al.*, 2003] indicate that the air from the probed layer has encountered fire events on 8 and 9 May in southern Manitoba and Saskatchewan, and weaker events in Belgium on 19 May, with no precipitation along the trajectory. A constant or slightly decreasing single-scattering albedo is also reported for polluted and biomass burning cases [*Bergstrom et al.*, 2007].

5.3. ARCTAS/ARCPAC, Alaska 2008

[37] Two SSFR systems were deployed in two coordinated campaigns in Alaska, 2008. One was mounted on the NASA P-3 (call sign N426NA) that participated in the ARCTAS experiment, the second on the NOAA WP-3 (call sign N43RF) in the ARCPAC experiment. The SSFR measured the irradiance on both aircraft, while the actinic flux density data was provided by the AFSR on the NOAA WP-3 aircraft. The missing actinic flux density at the altitude of the NASA-P3 was obtained from the radiative transfer model which was tested with the other three radiation measurements and agreed with them within the range of the measurement uncertainty. This was necessary to be able to study this case, but not critical because the retrieval uncertainty is dominated by net irradiance, not the actinic flux density (see section 4.3). On 15 April 2008, both aircraft performed coordinated flights with the NOAA WP-3 flying above an aerosol layer, and the NASA P-3 flying below the layer. In addition, the vertical profile of the aerosol extinction coefficient was measured simultaneously by an HSRL aboard a B200 aircraft [*Hair et al.*, 2008]. This was the only occurrence when measurements were taken from two aircraft at the same location and time, an advantage over the other two experiments described above, but the low optical depth of the probed aerosol layer poses a challenge. The probed aerosol is mostly Arctic haze caused by biomass burning aerosol from Siberian forest fires [*Warneke et al.*, 2009] mixed with ice (about 20% of AOD) [*Ferrare et al.*, 2009].

[38] The measurements were taken at 2000 UTC at 64.804°N, 156.170°W with the NASA P-3 at 2919 m altitude AGL and the NOAA P-3 at 5346 m. The solar zenith angle was 60.1°. The ozone column reported by OMI amounts to 429 DU. The AOD of the layer between these altitudes was only 0.05, as determined from the HSRL

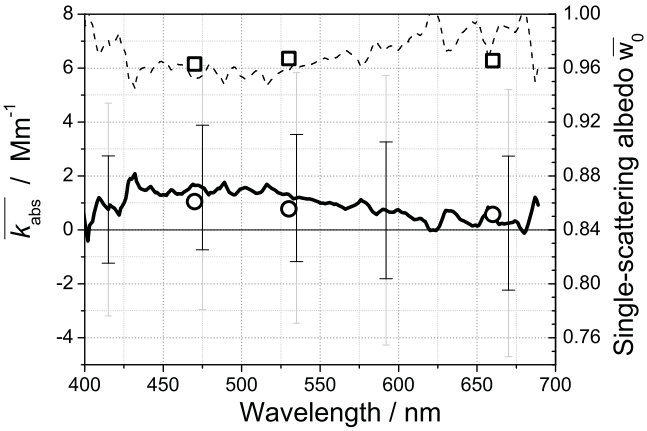

Figure 9. Retrieved mean absorption coefficient (solid line) and single-scattering albedo (dashed line) derived from ARCTAS/ARCPAC radiation measurements on 15 April 2008, west of Fairbanks, Alaska. The circles and squares show the absorption coefficient and single-scattering albedo, respectively, derived from HIGEAR PSAP and nephelometer measurements aboard the NASA P-3 in the same layer 1 h later.

extinction coefficient. Although this is even less than in the INSPECTRO United Kingdom case which yielded no absorption, the difference between the net irradiance at both levels was 3%–5% which is just at the limit of measurement uncertainty. The signal was larger than in the United Kingdom case because the aerosol is a stronger absorbing type, and this case is a crucial test of our new method, with the net irradiance difference just at the limit of instrument accuracy. The retrieved mean absorption coefficient of the probed aerosol layer is low, at less than 2 Mm^{-1} (Figure 9). The error bars are much larger than the absorption coefficient itself, because the vertical difference in net irradiances is low (less than 5%). However, the $\overline{k_{abs}}$ curve is very close to the in situ values measured at 2109 UTC within the same layer at 4.7 km flight altitude onboard the NASA P-3 (3 wavelength PSAP) which indicates that our new method yields sensible results even in this difficult case of low AOD. Nevertheless, the large error bars remind us how sensitive the retrieval is, in particular, to the quality of the irradiance measurements. The Absorption Ångström Exponent is 1.7 (470 and 660 nm) which is in the range of values for biomass burning aerosol given by *Bergstrom et al.* [2007].

6. Discussion

[39] An alternative approach to derive the absorption coefficient of aerosol particles from airborne radiation measurements has been tested and applied to data from a broad set of experimental conditions that provided a range of strong and weak signals. The mineral dust aerosol that was probed in Morocco during SAMUM provided a strong absorption signal, because of high optical depths in the vicinity of the dust sources. The first INSPECTRO experiment took place in an almost pristine environment on the English coast of East Anglia, and our method detected no aerosol absorption. The second INSPECTRO experiment in southern Germany, however, was accompanied by more substantial aerosol loading and our new method yielded a moderate absorption signal. The combined ARCTAS/ARCPAC experiment in Alaska was different in that irradiance was measured simultaneously from two aircraft at two altitudes. Although the probed AOD is low, the retrieved mean absorption coefficient compares very well to in situ measurements.

[40] In summary, we have found a confirmation of the hypothesis stated in section 4.3: the new method succeeded whenever the change in net irradiance between the two measurement levels was equal or higher than the measurement uncertainty for net irradiance of the instrument in use. The case in which that difference was about equal to the measurement uncertainty (the Alaska case) was particularly useful (albeit difficult to evaluate because of the unstabilized irradiance inlets) to validate this. The retrieval did succeed with results that compare well to independent in situ methods. The hypothesis is further strengthened by the United Kingdom 2002 case: although the AOD of the probed layer was even higher than in Alaska, the net irradiance change was well below the measurement uncertainty and consequently the retrieval yielded a result that was not significantly different from zero. While the reason is mainly the different aerosol type (less absorbing), this shows us that the AOD alone cannot be used as an indicator whether the new retrieval method will succeed or not. Nevertheless, this case is a positive null test for the aforementioned hypothesis. The German pollution case (2004) is the least conclusive one due to the lack of independent measurements.

[41] The presented method is somewhat limited in its applicability not only by the efforts it takes to perform the required airborne measurements of irradiance and actinic flux density but also in the high uncertainties involved because of the numerical delicacy when analyzing the small difference of large numbers that both have a certain absolute uncertainty. However, given the good agreement between the retrieval results and independent in situ measurements, with great experimental care and calibration efforts it seems possible to obtain useful results despite large error bars.

[42] It would be desirable to go a step further in future experiments and extend the actinic flux density measurements beyond 700 nm into the near infrared (up to 2.5 microns), as it has been done for irradiance measurements. The limiting factor is currently the lack of an optical sensor for actinic flux density that has useful transmission properties at such wavelengths. The efforts for actinic flux density detection have so far been focused on the visible and especially on the ultraviolet part of the spectrum, because the prevailing application has been the derivation of molecular dissociation rates for which the NIR is not significant.

[43] The new method proposed in this paper is, however, an application that might serve as an incentive for such an all-spectrum actinic flux density detector, as it enables measurement-based analyses of the absorption properties of atmospheric layers, regardless if the layers contain aerosol, clouds, or absorbing gases.

[44] Once a full solar spectrum of the actinic flux density is available, the spectral integral would furthermore open the possibility to calculate the (solar) heating rates of any atmospheric layer on the basis of measurements. Addition-

ally, the absorption coefficient at 750 nm would help to distinguish hematite from other minerals in dust aerosol because of its unique spectral absorption properties [*Müller et al.*, 2009].

[45] **Acknowledgments.** The authors are grateful to all field campaign participants who made the experiments possible, especially the aircraft operators, pilots, and coordinators. The field campaigns were supported by the German Research Foundation (Research Group SAMUM), NASA (ARCTAS), and NOAA (ARCPAC). Analyses used in this paper were produced with TOMS data from the Giovanni online data system, developed and maintained by the NASA Goddard Earth Sciences (GES) Data and Information Services Center (DISC).

References

Bergstrom, R., P. Pilewskie, B. Schmid, and P. Russell (2003), Estimates of the spectral aerosol single scattering albedo and aerosol radiative effects during SAFARI 2000, *J. Geophys. Res.*, *108*(D13), 8474, doi:10.1029/2002JD002435.

Bergstrom, R. W., P. Pilewskie, P. B. Russell, J. Redemann, T. C. Bond, P. K. Quinn, and B. Sierau (2007), Spectral absorption properties of atmospheric aerosols, *Atmos. Chem. Phys.*, *7*, 5937–5943.

Bierwirth, E. (2008), Airborne measurements of the spectral surface albedo over Morocco and its influence on the radiative forcing of Saharan dust, Ph.D. thesis, Johannes Gutenberg Univ. Mainz, Mainz, Germany.

Bierwirth, E., et al. (2009), Spectral surface albedo over Morocco and its impact on radiative forcing of Saharan dust, *Tellus, Ser. B*, *61*, 252–269.

Bond, T., T. Anderson, and D. Campbell (1999), Calibration and intercomparison of filter-based measurements of visible light absorption by aerosols, *Aerosol Sci. Technol.*, *30*, 582–600.

Chandrasekhar, S. (1960), *Radiative Transfer*, Dover, New York.

Chin, M., R. Kahn, and S. Schwartz (2009), *CCSP 2009: Atmospheric Aerosol Properties and Climate Impacts*, Natl. Aeronaut. and Space Admin., Washington, D. C.

Coddington, O., K. Schmidt, P. Pilewskie, W. Gore, R. Bergstrom, M. Román, J. Redemann, P. Russell, J. Liu, and C. Schaaf (2008), Aircraft measurements of spectral surface albedo and its consistency with ground-based and space-borne observations, *J. Geophys. Res.*, *113*, D17209, doi:10.1029/2008JD010089.

Crowther, B. (1997), The design, construction, and calibration of a spectral diffuse/global irradiance meter, Ph.D. thesis, Univ. of Ariz., Tucson.

Esselborn, M., M. Wirth, A. Fix, B. Weinzierl, K. Rasp, M. Tesche, and A. Petzold (2009), Spatial distribution and optical properties of Saharan dust observed by airborne high spectral resolution lidar during SAMUM 2006, *Tellus, Ser. B*, *61*, 131–143.

Draxler, R. R., and G. D. Hess (1998), An overview of the HYSPLIT 4 modelling system for trajectories, dispersion and deposition, *Aust. Meteorol. Mag.*, *47*, 295–308.

Ferrare, R., et al. (2009), NASA B-200 King Air operations and science during ARCTAS, paper presented at ARCTAS Workshop, Natl. Aeronaut. and Space Admin., Virginia Beach, Va., 27–30 Jan.

Früh, B., T. Trautmann, M. Wendisch, and A. Keil (2000), Comparison of observed and simulated NO_2 photodissociation frequencies in a cloudless atmosphere and in continental boundary layer clouds, *J. Geophys. Res.*, *105*, 9843–9857.

Gao, R., S. Hall, W. Swartz, J. Schwarz, J. Spackman, L. Watts, D. Fahey, K. Aikin, R. Shetter, and T. Bui (2008), Calculations of solar shortwave heating rates due to black carbon and ozone absorption using in situ measurements, *J. Geophys. Res.*, *113*, D14203, doi:10.1029/2007JD009358.

Giglio, L., J. Descloitres, C. O. Justice, and Y. Kaufman (2003), An enhanced contextual fire detection algorithm for MODIS, *Remote Sens. Environ.*, *87*, 273–282.

Gobbi, G., F. Barnaba, R. Giorgi, and A. Santacasa (2000), Altitude-resolved properties of a Saharan dust event over the Mediterranean, *Atmos. Environ.*, *34*, 5119–5127.

Hair, J., C. Hostetler, A. Cook, D. Harper, R. Ferrare, T. Mack, W. Welch, L. Izquierdo, and F. Hovis (2008), Airborne high spectral resolution lidar for profiling aerosol optical properties, *Appl. Opt.*, *47*, 6734–6752.

Haywood, J., P. Francis, I. Geogdzhayev, M. Mishchenko, and R. Frey (2001), Comparison of Saharan dust aerosol optical depths retrieved using aircraft mounted pyranometers and 2-channel AVHRR algorithms, *Geophys. Res. Lett.*, *28*, 2393–2396.

Heintzenberg, J. (2009), The SAMUM-1 experiment over southern Morocco: Overview and introduction, *Tellus, Ser. B*, *61*, 2–11.

Hudson, R., J.-H. Kim, and A. Thompson (1995), On the derivation of tropospheric column ozone from radiances measured by the total ozone mapping spectrometer, *J. Geophys. Res.*, *100*, 11,137–11,145.

Intergovernmental Panel on Climate Change (2007), Summary for policymakers, in *Climate Change 2007: The Physical Science Basis. Contribution of Working Group I to the Fourth Assessment Report of the Intergovernmental Panel on Climate Change*, edited by S. Solomon et al., pp. 1–18, Cambridge Univ. Press, New York.

Jäkel, E., M. Wendisch, A. Kniffka, and T. Trautmann (2005), Airborne system for fast measurements of upwelling and downwelling spectral actinic flux densities, *Appl. Opt.*, *44*, 434–444.

Jäkel, E., M. Wendisch, and B. Lefer (2006), Parameterization of ozone photolysis frequency in the lower troposhere using data from photodiode array detector spectrometers, *J. Atmos. Chem.*, *54*, 67–87.

Kanaya, Y., Y. Kajii, and H. Akimoto (2003), Solar actinic flux and photolysis frequency determinations by radiometers and a radiative transfer model at Rishiri Island: Comparisons, cloud effects, and detection of an aerosol plume from Russian forest fires, *Atmos. Environ.*, *37*, 2463–2475.

Kandler, K., et al. (2009), Size distribution, mass concentration, chemical and mineralogical composition and derived optical properties of the boundary layer aerosol at Tinfou, Morocco, during SAMUM 2006, *Tellus, Ser. B*, *61*, 32–50.

Knippertz, P., et al. (2009), Dust mobilization and transport in the northern Sahara during SAMUM 2006—A meteorological overview, *Tellus, Ser. B*, *61*, 12–31.

Kokhanovsky, A., et al. (2007), Aerosol remote sensing over land: A comparison of satellite retrievals using different algorithms and instruments, *Atmos. Res.*, *85*, 372–394.

Kylling, A., et al. (2005), Spectral actinic flux in the lower troposphere: Measurement and 1-D simulations for cloudless, broken cloud and overcast situations, *Atmos. Chem. Phys.*, *5*, 1975–1997.

Levelt, P. F., G. H. J. van den Oord, M.R. Dobber, A. Mälkki, H. Visser, J. de Vries, P. Stamnes, J. O. V. Lundell, and H. Saari (2006), The Ozone Monitoring Instrument, *IEEE Trans. Geosci. Remote Sens.*, *44*, 1093–1101.

Liu, Y., J. R. Key, and X. Wang (2008), The influence of changes in cloud cover on recent surface temperature trends in the arctic, *J. Clim.*, *21*, 705–715.

Mayer, B. and A. Kylling (2005), Technical note: The libRadtran software package for radiative transfer calculations - description and examples of use. *Atmos. Chem. Phys.*, *5*, 1855–1877.

Müller, T., A. Schladitz, A. Maßling, N. Kaaden, K. Kandler, and A. Wiedensohler (2009), Spectral absorption coefficients and imaginary parts of refractive indices of Saharan dust during SAMUM-1, *Tellus, Ser. B*, *61*, 79–95.

Otto, S., E. Bierwirth, B. Weinzierl, K. Kandler, M. Esselborn, M. Tesche, A. Schladitz, M. Wendisch, and T. Trautmann (2009), Solar radiative effects of a Saharan dust plume observed during SAMUM assuming spheroidal model particles, *Tellus, Ser. B*, *61*, 270–296.

Pilewskie, P., J. Pommier, R. Bergstrom, W. Gore, S. Howard, M. Rabbette, B. Schmid, P. V. Hobbs, and S. C. Tsay (2003), Solar spectral radiative forcing during the Southern African Regional Science Initiative, *J. Geophys. Res.*, *108*(D13), 8486, doi:10.1029/2002JD002411.

Redemann, J., P. Pilewskie, P. B. Russell, J. M. Livingston, S. Howard, B. Schmid, J. Pommier, W. Gore, J. Eilers, and M. Wendisch (2006), Airborne measurements of spectral direct aerosol radiative forcing in the Intercontinental chemical Transport Experiment/Intercontinental Transport and Chemical Transformation of anthropogenic pollution, 2004, *J. Geophys. Res.*, *111*, D14210, doi:10.1029/2005JD006812.

Schladitz, A., T. Müller, N. Kaaden, A. Maßling, K. Kandler, M. Ebert, S. Weinbruch, C. Deutscher, and A. Wiedensohler (2009), In situ measurements of optical properties at Tinfou (Morocco) during the Saharan Mineral Dust Experiment SAMUM 2006, *Tellus, Ser. B*, *61*, 64–78.

Schmidt, K. S., G. Feingold, P. Pilewskie, H. Jiang, O. Coddington, and M. Wendisch (2009), Irradiance in polluted cumulus fields: Measured and modeled cloud-aerosol effects, *Geophys. Res. Lett.*, *36*, L07804, doi:10.1029/2008GL036848.

Stamnes, K., S. Tsay, W. Wiscombe, and K. Jayaweera (1988), A numerically stable algorithm for discrete-ordinate-method radiative transfer in multiple scattering and emitting layered media, *Appl. Opt.*, *27*, 2502–2509.

Stark, H., B. Lerner, R. Schmitt, R. Jakoubek, E. Williams, T. Ryerson, D. Sueper, D. Parrish, and F. Fehsenfeld (2007), Atmospheric in situ measurement of nitrate radical (NO_3) and other photolysis rates using spectroradiometry and filter radiometry, *J. Geophys. Res.*, *112*, D10S04, doi:10.1029/2006JD007578.

Thiel, S., et al. (2008), Influence of clouds on the spectral actinic flux density in the lower troposphere (INSPECTRO): Overview of the field campaigns, *Atmos. Chem. Phys.*, *8*, 1789–1812.

Virkkula, A., N. Ahlquist, D. Covert, W. Arnott, P. Sheridan, P. Quinn, and D. Coffman (2005), Modification, calibration and a field test of an instrument for measuring light absorption by particles, *Aerosol Sci. Technol.*, *39*, 68–83.

von Hoyningen-Huene, W., T. Dinter, A. Kokhanovsky, J. Burrows, M. Wendisch, E. Bierwirth, D. Müller, and M. Diouri (2009), Measurements of desert dust optical characteristic at Porte au Sahara during SAMUM, *Tellus, Ser. B*, *61*, 206–215.

Warneke, C., et al. (2009), Biomass burning in Siberia and Kazakhstan as an important source for haze over the Alaskan Arctic in April 2008, *Geophys. Res. Lett.*, *36*, L02813, doi:10.1029/2008GL036194.

Webb, A. R., A. Kylling, M. Wendisch, and E. Jäkel (2004), Airborne measurements of ground and cloud spectral albedos under low aerosol loads, *J. Geophys. Res.*, *109*, D20205, doi:10.1029/2004JD004768.

Wendisch, M., S. Mertes, A. Ruggaber, and T. Nakajima (1996), Vertical profiles of aerosol and radiation and the influence of a temperature inversion: Measurements and radiative transfer calculations, *J. Appl. Meteorol.*, *35*, 1703–1715.

Wendisch, M., D. Müller, D. Schell, and J. Heintzenberg (2001), An airborne spectral albedometer with active horizontal stabilization, *J. Atmos. Oceanic Technol.*, *18*, 1856–1866.

Wendisch, M., P. Pilewskie, E. Jkel, S. Schmidt, J. Pommier, S. Howard, H. H. Jonsson, H. Guan, M. Schrder, and B. Mayer (2004), Airborne measurements of areal spectral surface albedo over different sea and land surfaces, *J. Geophys. Res.*, *109*, D08203, doi:10.1029/2003JD004392.

E. Bierwirth, A. Ehrlich, and M. Wendisch, Leipziger Institut für Meteorologie, Universität Leipzig, Stephanstr. 3, D-04103 Leipzig, Germany. (eike.bierwirth@gmx.de)

A. Clarke, School of Ocean and Earth Science and Technology, University of Hawai'i at Mānoa, 1000 Pope Rd., MSB 506, Honolulu, HI 96822, USA.

M. Esselborn, Institut für Physik der Atmosphäre, Deutsches Zentrum für Luft- und Raumfahrt, Münchner Str. 20, D-82234 Oberpfaffenhofen, Germany.

R. Ferrare, NASA Langley Research Center, Mail Stop 401A, Hampton, VA 23681, USA.

G. P. Gobbi, Institute of Atmospheric Sciences and Climate, CNR, Via Fosso del Cavaliere 100, I-00133 Rome, Italy.

E. Jäkel, Institute for Atmospheric Physics, Johannes Gutenberg University Mainz, Becherweg 21, D-55099 Mainz, Germany.

T. Müller, Leibniz Institute for Tropospheric Research, D-04318 Leipzig, Germany.

P. Pilewskie and K. S. Schmidt, Laboratory for Atmospheric and Space Physics, University of Colorado, Campus Box 392 UCB, Boulder, CO 80309, USA.

H. Stark, Earth System Research Laboratory, NOAA, 325 Broadway, Boulder, CO 80305, USA.